Density Functional Study of the Anionic Hypoxanthine Tautomeric Forms

ARTICLE *in* JOURNAL OF MOLECULAR STRUCTURE THEOCHEM · MARCH 2000

Impact Factor: 1.37 · DOI: 10.1016/S0166-1280(99)00278-X

ELSEVIER

Journal of Molecular Structure (Theochem) 499 (2000) 71–84

THEO CHEM

www.elsevier.nl/locate/theochem

Density functional study of the anionic hypoxanthine tautomeric forms

M.E. Costas[a,*], R. Acevedo-Chávez[b]

[a]*Facultad de Química, Universidad Nacional Autónoma de México, México 04510 D.F., Mexico*
[b]*Centro de Química, Instituto de Ciencias, B. Universidad Autónoma de Puebla, Apartado Postal 1613, Puebla, Mexico*

Received 28 June 1999; accepted 14 July 1999

Abstract

Chemical and physicochemical properties of certain purine derivatives and isomers have been studied for several years. One of these heterocycles, hypoxanthine (hyp), has focused our attention under systematically modified protonation levels and tautomeric and isomeric forms. In the study reported here, we have carried out the Density Functional Theory calculations for all the possible tautomeric forms of monoanionic and dianionic hypoxanthine. For these, we have obtained: (i) the total molecular energies; (ii) several molecular and electronic structure properties; (iii) the $\Delta\bar{G}$ values associated with heterocyclic tautomeric equilibria and monoprotonation processes; and (iv) the IR vibrational spectra. From the study, the relationship between the theoretical properties and both the anionic state and tautomeric forms arise. Among the results obtained, we found that the N(1)–H ketonic form is the comparatively most stable hypoxanthine^{1-} species. Considering previous theoretical calculations, the suggested descending sequence of π-type reductor character is: $hyp^{2-} > hyp^{1-} > hyp^{0} > hyp^{1+} > hyp^{2+} > hyp^{3+}$. Also, the suggested descending sequence of σ-type basicity is: N(1) > N(9) ≈ N(7) > N(3) > 0. The theoretical study supports both the N(1)–H predominance in hyp^{1-} aqueous solutions and the experimental reactivity of anionic hypoxanthine. All the suggested trends are in very good concordance with the experimental physicochemical and chemical behavior of hypoxanthine in different protonation states.

Keywords: Hypoxanthine; Tautomers; Theoretical calculations; Density functional theory calculations

1. Introduction

Heterocycles showing in their structures pyrimidinic rings fused to azolic moieties are interesting systems from the biochemical, pharmacological, chemical and physicochemical points of view [1–5]. One member of this family, hypoxanthine (Fig. 1), is found as a minor purine base in transfer RNA [2,3].

In the purines catabolism hypoxanthine is catalitically oxidized by the metalloenzyme xanthine oxidase in the production of uric acid [1,2]. Regarding the hypoxanthine physicochemical and chemical properties, several experimental studies have been carried out on the hypoxanthine–transitional Lewis acid (L–M) interactions. In these, the N atoms have been found to be the favored metallic coordination sites, their identity being strongly dependent on the experimental reaction conditions [3,4,6]. The hypoxanthine–H^+ $(L–H)^+$ interactions have also been explored [7–16]. Nevertheless, there is no evidence of a clear relationship between the L–M and the L–H^+ thermodynamic stabilities in which a common electron-donor N site is involved. In addition, in all these hypoxanthine–Lewis acid interactions the

* Corresponding author.

0166-1280/00/$ - see front matter
PII: S0166-1280(99)00278-X

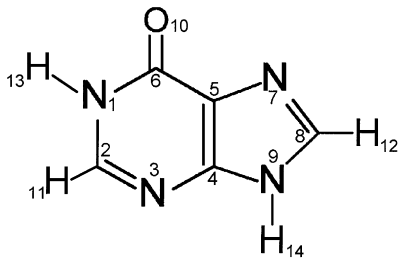

Fig. 1. Schematic drawing and numbering sequence for the structure of neutral hypoxanthine in its N(1)–H/N(9)–H ketonic tautomeric form.

heterocyclic tautomerism appears to play a critical role. The prototropic tautomerism has been deduced from experimental studies on neutral hypoxanthine in solution [10,17,18], and the N(1)–H/N(9)–H and the N(1)–HN(7)–H ketonic tautomers have been considered as the predominant forms. These two tautomers have also been proposed as the most stable ones from theoretical studies [19]. In spite of these advances, the tautomerism and isomerism in anionic hypoxanthine have not yet been explored systematically, either experimentally or theoretically. Also, the possible relationship between the hypoxanthine^{n-} protonation state with its physicochemical and chemical properties has not been thoroughly studied.

As these problems are of our interest, we performed exhaustive and systematic theoretical calculations at the DFT level for all the six possible monoanionic tautomers and the dianionic form of hypoxanthine. In this paper, we present and discuss: (i) the relative energetic stabilities; (ii) several molecular and electronic structure properties; (iii) the tautomeric equilibrium constants; (iv) the heterocyclic monoprotonation $\Delta\bar{G}$ values; and (v) the IR vibrational spectra of both the most stable monoanionic form and the dianionic state. Trends for some properties as a function of the heterocyclic protonation level and tautomerism or isomerism are also found. These trends could contribute to analyze some aspects of the physicochemical and chemical behavior of hypoxanthine both in gas phase and condensed state.

2. Methodology

The calculations for full geometry optimizations, total molecular energies and several molecular and electronic structure properties for the six possible monoanionic forms and the dianionic state of hypoxanthine (Fig. 2) were performed at the Density Functional Theory level. The Becke–Perdew functional [20,21] and the DZVP basis set [22] were employed using the standard procedure in Gaussian 94 [23].

We also performed tests (full geometry optimizations, total molecular energies and frequency calculations) with different functionals (BP, BLYP and B3LYP) and basis sets (DZVP, 6-31G and 6-31G**) for the monoanionic species, as much has been discussed about the difficulty of studying anionic systems [24–26] and tautomeric equilibria [27] by DFT methods. As will be discussed in Section 3, the identity of the most stable monoanionic tautomeric

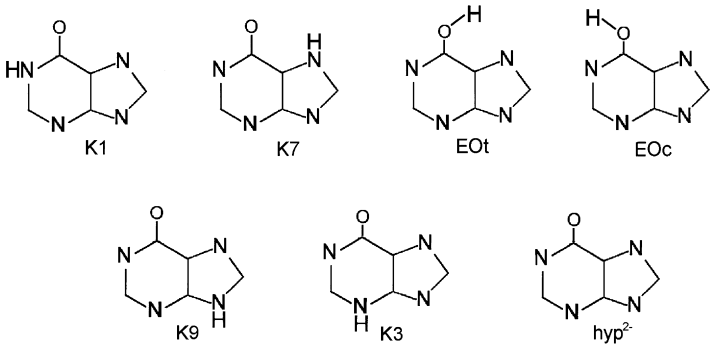

Fig. 2. Schematic drawing of both the six possible hypoxanthine monoanionic forms and hypoxanthine^{2-} (hyp^{2-}). The number in K (ketonic) tautomers refer to the endocyclic prototropic tautomerism H atom position. EOt and EOc correspond in the enolic forms to the *trans*- and *cis*-OH group configuration relative to the N(1) atom, respectively.

Table 1
Relative total molecular energies (kcal/mol) for the K7 and EOt hypoxanthine^{1-} monoanionic tautomers referred to the most stable K1 form, calculated with different functionals and basis sets. Zero-point energy is included in the total molecular energies

Tautomer	BP86/DZVP	BP86/6-31G	BP86/6-31G**	BLYP/DZVP	B3LYP/DZVP
K1	–	–	–	–	–
EOt	3.90	3.30	3.64	4.17	3.16
K7	3.75	4.92	5.38	3.86	3.46

form was the same for all the different calculation levels. We think that in our case, the inherent problems found in DFT methods for anionic systems are non existent, because here the anionic forms we calculate are closed shell (i.e. they are formed by eliminating one or two hydrogen nuclei ($\underline{H}^+$) and not introducing additional electrons). In addition, for the most stable monoanionic tautomer, the structural parameters (distances and angles) were within a deviation of 0.5% for all the different calculations, and the other properties (e.g. electronic charge density, frontier molecular orbitals symmetry, electric dipole moment vector and electrostatic potential) were the same.

Finally, we have confidence in DFT calculations due to the very good results obtained for neutral hypoxanthine [19] in comparison with the experimental data. In consequence, we decided to continue the systematic study we are doing on ionic hypoxanthine employing the Becke–Perdew functional and the DZVP basis set.

The optimized structures of the neutral hypoxanthine tautomeric forms [19] were used as input data to construct all the anionic forms for the geometry optimization procedure. The construction was made by eliminating one and two hydrogen nuclei ($\underline{H}^+$). Criteria for geometry optimization and SCF-convergence were 10^{-7} hartree/bohr and 10^{-9} hartree, respectively. Frequency calculations were performed to establish the nature of the stationary points found by geometry optimizations. All the anionic forms were stationary points in the geometry optimization procedure, and none showed imaginary frequencies in the vibrational analysis.

All the full optimized geometries were used to perform single-point calculations with GAUSSIAN 92 [28], in order to visualize several molecular and electronic structure properties. The difference between the SCF-energy and the value obtained with GAUSSIAN 94 was of 10^{-8} hartree in all cases. Visualization of the several calculated properties was carried out with the UNICHEM program [29]. Single-point calculations with the DGAUSS program [30] for the GAUSSIAN 94 optimized geometries were also done to obtain the Mayer valence indices [31].

The calculated frequencies (as wave numbers) of the IR vibrational spectra absorptions were corrected with a scaling factor of 1.0054. This value was obtained by comparing the theoretical IR ν(C=O) vibrational mode wave number (1725.6988 cm^{-1}) for the $\underline{N}$(1)–H/$\underline{N}$(7)–H hypoxanthine tautomer in gas phase with the experimental value (1735 cm^{-1}) [32]. Assignment of the vibrational normal modes for the different anionic forms was made by visualizing them at each frequency value with the XMOL 1.3.1 program [29]. Frequency calculations were performed at 298.15 and 480.15 K to obtain the molar Gibbs free energy thermal corrections. The contributions to these corrections were calculated within the rigid rotor-harmonic oscillator-ideal gas approximation with the rotational constants and harmonic frequencies using the standard methods of statistical mechanics [33]. From these $\bar{G}$ values, the constants of the tautomeric equilibria and the $\Delta\bar{G}$ values for the heterocyclic monoprotonic transfer processes at the two different temperatures were calculated. The first vertical ionization potential and the first vertical electron affinity were obtained from calculations of the SCF-energy for the resulting radicals (at the same optimized structures of the, respectively, starting anionic forms).

The calculations were done on an Origin SG1-2000 and a CRAY YMP4/464 supercomputers (at DGSCA, UNAM) and a SG1-R4400 workstation (at FQ, UNAM).

Table 2
(a) Internuclear distances (Å), (b) Angles (degree), and (c) Mayer valence-occupied indices for the hypoxanthine^{1-} N(1)–H tautomeric form (K1) and hypoxanthine^{2-} (hyp^{2-})

Group/atom	K1	hyp^{2-}
(a) Group		
N1–C2	1.387	1.356
C2–N3	1.311	1.350
N3–C4	1.389	1.387
C4–C5	1.441	1.432
C5–C6	1.441	1.463
C6–N1	1.441	1.413
C5–N7	1.379	1.399
N7–C8	1.359	1.360
C8–N9	1.370	1.372
N9–C4	1.368	1.388
C6–O10	1.254	1.279
C2–H11	1.100	1.114
C8–H12	1.098	1.105
N1–H13	1.023	–
(b) Group		
N1–C2–N3	124.68	131.96
C2–N3–C4	113.42	110.67
N3–C4–C5	125.64	124.28
C4–C5–C6	120.66	120.04
C5–C6–N1	109.31	114.26
C6–N1–C2	126.29	118.78
C4–C5–N7	109.15	108.79
C5–N7–C8	101.45	101.44
N7–C8–N9	118.49	118.93
C8–N9–C4	101.62	101.02
N9–C4–C5	109.28	109.82
N3–C4–N9	125.08	125.90
C6–C5–N7	130.19	131.17
N1–C6–O10	118.29	120.25
C5–C6–O10	132.40	125.48
N1–C2–H11	115.34	114.02
N3–C2–H11	119.98	114.02
N7–C8–H12	120.88	120.68
N9–C8–H12	120.63	120.39
C2–N1–H13	119.82	–
C6–N1–H13	113.88	–
(c) Atom		
N1	3.239	3.070
C2	3.999	4.197
N3	3.211	3.121
C4	4.043	4.118
C5	3.945	3.952
C6	4.231	4.424
N7	3.124	3.114
C8	4.052	4.070
N9	3.102	3.088
O10	2.143	2.029
H11	0.916	0.919
H12	0.927	0.931
H13	0.872	–

3. Results and discussion

In this section we will mainly present the properties for both the most stable monoanionic tautomer and hypoxanthine^{2-}. However, some trends that include less stable monoanionic forms will be discussed. General trends for some properties that consider other hypoxanthine protonation states will be also commented.

3.1. Relative energetic stability

Table 1 shows the relative energies for the three most stable hypoxanthine^{1-} tautomers.

The relative energetic stability order we found when the zero-point energy is not considered was K1 > EOt > K7 for all the different calculations. When this energy is included, the relative energetic stability order of the enolic-*trans* (EOt) and the N(7)–H (K7) tautomers changed in some calculations. In both cases the N(1)–H (K1) form is the comparatively most stable one. As the energetic difference between the EOt and the K7 tautomers is less than 2 kcal/mol in all the cases, nothing can be assured about the reliability of the relative stability order for these two tautomers. At this calculation level, the suggestion about the possible coexistence of the three monoanionic tautomers in the gas phase can be made. We also did the analysis of the $\Delta\bar{G}$ values considering the most stable species and the following two tautomers for all the basis sets and functionals explored. The same stability order than that obtained from the corresponding total molecular energies analysis was found in all the cases.

For hypoxanthine^{1-}, the possible influence of the imidazolic ring deprotonation state on the stabilization of certain tautomers could be suspected. For both the neutral [19] and monoanionic hypoxanthine, the most stable tautomers belong to the N(1)–H ketonic form. These results could suggest that the neutral hypoxanthine deprotonation process in the gas phase is characterized mainly by the predominance of the N(1)–H (K1) ketonic form in the resulting monoanionic heterocycle. At this level of study, it is also possible to suggest that in the additional deprotonation of hypoxanthine^{1-}, the N(1) atom would be the electron-donor site mainly involved in the heterocyclic protonic dissociation. The total molecular energy

difference between hypoxanthine^{2-} and K1 is remarkable (431.71 kcal/mol), in concordance with the noticeable reluctance of the heterocycle to show a full N–H deprotonation (in fact, hypoxanthine^{2-} has only been obtained [7–16] in aqueous solution at very high pH values ($\geq$ 13)).

Regarding the experimental studies carried out on the characterization of hypoxanthine^{1-} in solution, the results and interpretations, in our opinion, are not yet conclusive. Two general propositions on the predominant monoanionic tautomeric forms have been elaborated: the first one [9,11,15] suggests the K7 and/or K9 tautomers existence (including in this the possibility of mesomeric forms). The second one [10] considers an ensemble of tautomeric and mesomeric equilibria, in which the deprotonation state of the imidazolic ring is the remarkable feature of the monoanionic forms; in their formation, the N(1)–H group protonic dissociation is discarded.

In this second scheme, the monoanionic forms considered as predominant are K1, an enolic form, K7 and K9 (including for these two last tautomers possible mesomeric forms). This proposition would be in considerable agreement with the theoretical energetic stability sequence commented before, and specially with the K1, EOt and K7 tautomers here suggested as the comparatively most stable ones in the gas phase. Also, this last experimental study would be in full agreement with our theoretical results and suggestion about the involvement of the N(1)–H group in K1 as the main protonic dissociation site in the hypoxanthine^{2-} formation.

3.2. Structural and valence-occupied parameters

Internuclear distances, angles and Mayer indices for the optimized structures of the monoanionic tautomers and dianionic hypoxanthine were analyzed. Table 2 shows the values for K1 and hypoxanthine^{2-}.

The influence of the N–H group position on the angles is found when the structural data for the hypoxanthine^{1-} tautomers are analyzed. Those N atoms which are protonated are involved in higher C–N–C group angles than the deprotonated ones. This behavior has also been found both in experimental [6] and theoretical studies [19] on neutral hypoxanthine–Lewis acid systems, in which the heterocycle shows prototropic tautomerism in the five-membered ring. This same structural pattern has been deduced from a theoretical analysis [34] for hypoxanthine^{1+} N(1)–H/N(7)–H/N(9)–H tautomer, and has been corroborated experimentally [35–38]. Theoretical calculations on dicationic [39] and tricationic [40] hypoxanthine have yielded analogous results.

Tautomerism influences the values of the C(5)–C(6)–0 and the N(1)–C(6)–0 angles. For the N(7)–H (K7) tautomer, the first angle is lower than the second one. This behavior could be related to the existence of attractive intramolecular interactions through the O···H–N(7) pair. In some measure, this suggestion could be supported through the behavior of the same angles in the EOt and EOc tautomers. In these, the O–H group would appear to be involved in attractive N···H–O interactions.

With regard to the six- and five-membered rings symmetry, this is higher in the last one, and is particularly noticeable in the cases where the imidazolic ring is deprotonated. In such cases, the angles of the two C–N–C groups are very similar. This structural behavior could be associated with a comparatively higher electronic charge density delocalization throughout that ring.

Tautomerism also influences the internuclear distances. Those N atoms that are deprotonated are involved in lower internuclear distances with their neighboring C atoms. This same behavior is found in the C(6)–O group when the exocyclic atom shows deprotonation. In those cases, a double-bond character is suggested to be associated with such comparatively lower internuclear distances.

This internuclear distance behavior has also been found in the theoretical [19,34,39,40] and experimental [6,35–38] studies above quoted. The Mayer valence-occupied indices values are in agreement with the above theoretical suggestion and those experimental studies. The dihedral angles obtained for the monoanionic forms, let us consider that in all the cases the structures show full planarity.

On the other hand and for hypoxanthine^{2-}, both the C–N–C angles similarity in the imidazolic ring, the double-bend character for the C(6)–O group and N atoms which are deprotonated arise. These features are also in concordance with the Mayer indices values. The dihedral angles let us consider that also in this case the structural planarity is fully achieved.

3.3. Total electronic charge density

Fig. 3(a) shows the total electronic charge density (TECD) contour maps for K1 and hypoxanthine^{2-}.

For the lowest value (0.05), electronic communication throughout the structures is observed. However, differences are detected for higher values of the TECD. In particular, those molecular regions associated with lower internuclear distances and also the N and O atoms deprotonated, even show electronic communication. This is remarkable for example, in the C(6)–O and C–N groups, in which deprotonation of the heteroatoms is maintained. These features support both the double-bond character and the higher electronic charge density delocalization suggested before. The TECD features here commented follow an analogue pattern to those corresponding to the most stable neutral [19] and cationic [34,39,40] hypoxanthine species.

3.4. Molecular electrostatic potential and electric dipole moment

Fig. 3(b) and (c) show the molecular electrostatic potential (MEP) contour maps together with the electric dipole moment (EDM) vectors and the 3D-MEP, respectively, for both K1 and hypoxanthine^{2-}. The EDM vector magnitudes are 4.9 and 2.0 Debye for K1 and hypoxanthine^{2-}, respectively.

The influence of both tautomerism and anionic level on the MEP distribution around the molecules is remarkable. In these, both the O site and the N deprotonated atoms are associated with negative (attractive) values of the MEP. However, and for a particular MEP level, those heterocyclic features also influence the potential participation of these sites in attractive electrostatic interactions with Lewis acids. For example, and for the N(1)–H tautomer, the more favorable atoms are N(7) and N(9) at the −147 kcal/mol level. At this MEP value for hypoxanthine^{2-}, all the N sites and the O atom are favorable ones. Only at higher MEP levels, differences arise: for example and for the −250 kcal/mol level, the O site is now the unique potential favorable site.

On the contrary, those protonated groups are associated with repulsive electrostatic interactions. The MEP features discussed here are in full agreement with the EDM vector properties. The MEP and EDM vector properties follow analogous patterns to those found in the previously quoted theoretical studies [19,34,39,40].

3.5. HOMO and LUMO wave functions-energy and symmetry properties

The HOMO and LUMO wave functions energies for K1 are −0.84 and +2.70 eV, respectively. Fig. 4 shows its 3D-HOMO and LUMO wave functions.

When the frontier molecular orbitals energies for all the monoanionic tautomers are analyzed, a gross HOMO energies ascending trend relative to the descending tautomeric energetic stability is found. For the LUMO energies an increasing trend is first observed, and secondly a decrease is found. For hypoxanthine^{2-}, the HOMO and LUMO energies are +4.18 and +7.85 eV, respectively. Its 3D-wave functions are also shown in Fig. 4.

Comparison of the HOMO and LUMO energies for hypoxanthine^{2-} with those for the most stable forms of monoanionic (this study), neutral [19], monocationic [34], dicationic [39] and tricationic [40] hypoxanthine, let us suggest a theoretical descending sequence of reductor (Lewis base) character for the heterocycle: $hyp^{2-} > hip^{1-} > hyp^{0} > hyp^{1+} > hyp^{2+} > hyp^{3+}$. The opposite trend can be attributed to the oxidant (Lewis acid) character. These are in full qualitative agreement with the decreasing chemical reactivity experimentally shown up to the present date [6,35–38,41] by hypoxanthine towards Lewis acids (e.g. transitional metallic centers) upon its increasing protonation level.

The hypoxanthine^{1-} HOMO wave functions (π-type) molecular distribution is the same, independently of the monoanionic tautomeric form. These same features are also observed in the hypoxanthine^{2-} HOMO wave function (Fig. 4) and in neutral [19], monocationic [34], dicationic [39] and tricationic [40] hypoxanthine. This would mean that the identity of the potential π-type electron-donor sites associated with the HOMO wave function is non dependent of both the hypoxanthine protonation level and its tautomeric or isomeric form. In consequence, it is possible to postulate that in the heterocyclic Lewis base (L) reactivity towards homologous π-type Lewis acid (M) species, the initial formation of a M − L chemical

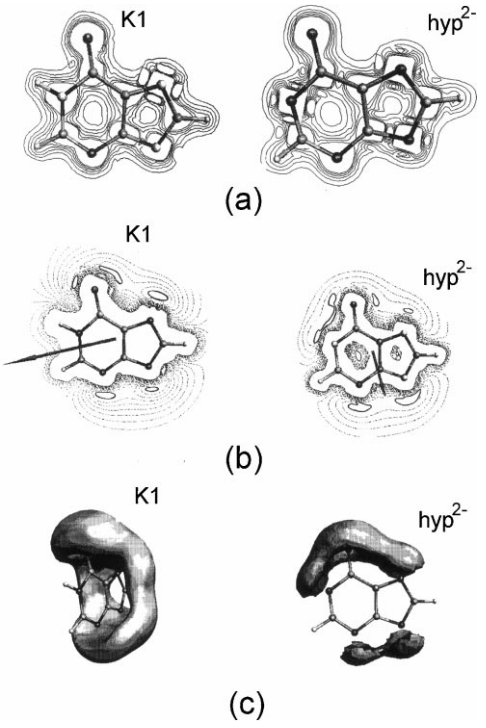

Fig. 3. (a) TECD contour maps at the molecular plane (0.05–0.3 e/Å^3 range, changes in 0.05 units), (b) negative (attractive) MEP contour maps at the molecular plane together with the EDM vector (referred to the molecular-center of mass and lying on the molecular plane), and (c) 3D-negative MEP for both the hypoxanthine^{1-} K1 tautomer and hypoxanthine^{2-}. 2D-MEP for K1 is in the 0 to −160 kcal/mol range, changes in 10 units; for hypoxanthine^{2-}, in the 0 to −250 kcal/mol range, changes in 20 units. The head of the arrow, which represents the EDM vector, points to the positive tip. MEP surfaces are −100 kcal/mol for K1 and −220 kcal/mol for the dianionic species.

bond would not require necessarily the heterocyclic potential electron-donor site deprotonation state. This postulate would be indirectly reflected, for example, through the experimental instability shown by hypoxanthine^{1+}-transition metallic compounds at very low (= 1.0) pH values [6], in which case the corresponding Metal–Ligand chemical interactions lead to stable neutral hypoxanthine-Cu(II) compounds. In here, although both groups, the N(7)–H and N(9)–H, exist in the hypoxanthine^{1+} free ligand, the Cu(II)–N(7) or Cu(II)–N(9) chemical bonds emerge in the resulting copper coordination compounds.

Finally, the LUMO wave functions are also π-type in all the hypoxanthine anionic forms. However, their molecular distribution is sensitive to the tautomeric form and heterocyclic deprotonation level. In consequence, the identity of the potential π-type electron-acceptor sites is dependent of the deprotonation level and the tautomeric form. An analogue behavior has also been found in the most stable forms of neutral [19], monocationic [34], dicationic [39] and tricationic [40] hypoxanthine.

3.6. Ionization potential and electron affinity

The first vertical ionization potential (IP) and electron affinity (EA) values for K1 are + 3.52 and +5.39 eV, respectively. These values correspond to the energetic difference for the processes: monoanionic species (S = 0) → neutral radical species (S = 1/2), and monoanionic species (S = 0) → dianionic radical species (S = 1/2), respectively. The IP and EA values for all the monoanionic tautomers are in full agreement with their HOMO and LUMO energies, respectively. The IP and EA values for K1 support both its stronger reductor and weaker oxidant properties above commented. In these K1 Redox processes, the MOs suggested to be mainly involved are the π-type HOMO and LUMO commented before, respectively.

For hypoxanthine^{2-}, the first vertical IP and EA values calculated belong to the energetic difference for the processes: dianionic species ($S = 0$) → monoanionic radical species ($S = 1/2$), and dianionic species ($S = 0$) → trianionic radical species ($S = 1/2$), respectively. For the first process, the total molecular energy for the resulting monoanionic radical species ($S = 1/2$) is 1.52 eV lower than for the starting dianionic one ($S = 0$). This supports the comparatively strongest hypoxanthine^{2-} reductor character quoted before. For the second process, the total molecular energy for the trianionic radical species ($S = 1/2$) is 10.36 eV higher than for the dianionic one ($S = 0$), also supporting the comparatively weakest hypoxanthine^{2-} oxidant character. In these Redox processes the MOs suggested to be mainly involved are the π-type HOMO and LUMO discussed before.

When considering the first vertical IP theoretical values for the most stable forms of tricationic [40], dicationic [39], monocationic [34], neutral [19], and monoanionic and dianionic hypoxanthine (this study), a clear relationship emerges: the IP increases with the

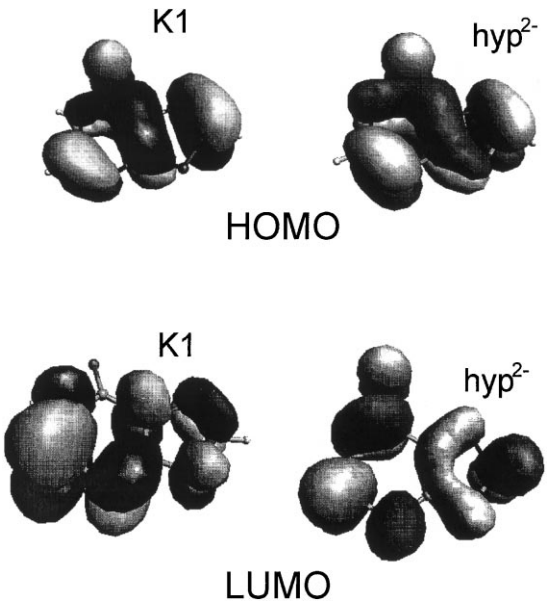

Fig. 4. HOMO and LUMO wave functions isosurfaces (± 0.025 level) for both the hypoxanthine^{1-} K1 tautomer and hypoxanthine^{2-}, respectively.

protonation level. This is, the heterocyclic reductor character descending sequence is the same as that inferred from the analysis in Section 3.5. The sequence here commented is the opposite one to that for the heterocyclic oxidant character, which is deduced from the relationship found between the theoretical EA values and the hypoxanthine protonation level.

The above theoretical trends are in full qualitative agreement with the hypoxanthine experimental reactivity [6,7–16,35–38,41] at different pH values in its chemical interactions with either $\underline{H}^+$ or transitional metallic centers (for example, hypoxanthine^{2-} is found as the strongest Lewis base and the weakest Lewis acid species; hypoxanthine^{3+} is the weakest Lewis base and the strongest Lewis acid species).

3.7. Tautomeric equilibria in the gas phase as a function of temperature

In the same way as for neutral [19] or cationic [34,39,40] hypoxanthine, an interesting aspect in the gas phase concerns to the monoanionic tautomeric equilibrium constants evaluation. We calculated the tautomeric constants corresponding to the equilibria: Tautomer K1⇔Tautomer *i*, for which

$$K_{eq} = \frac{[\text{Tautomer } i]}{[\text{Tautomer K1}]} = e^{-\Delta\bar{G}/RT}$$

where $\Delta\bar{G}$ is the molar Gibbs free energy difference between tautomer *i* and tautomer K1. Table 3(a) shows the K_{eq} values at two temperatures for the tautomeric equilibria involving all the possible monoanionic forms. We include all these forms in order to corroborate the monoanionic tautomers descending stability.

From this table and for a particular temperature, a K_{eq} values descending trend with the tautomers energetic stability is found. Here we observe that the main relative tautomeric population decreasing sequence is: K1 ≫ K7 > EOt. For a particular tautomeric equilibrium, the increase of temperature does not have a significant influence on the K_{eq} values. Interestingly, the K_{eq} values would also be in agreement with the experimental proposition [10] concerning the K1 predominant contribution in hypoxanthine^{1-} aqueous solutions.

3.8. Anionic hypoxanthine step-by-step protonation Gibbs free energies

We analyzed some hypoxanthine^{n-} protonation thermodynamic aspects, as for example, the heterocyclic electron-donor sites protonic affinities. The $\Delta\bar{G}$ values for such L–H$^+$ processes as a function of both the protonation step, the relative tautomeric energetic stability, the protonation site and the temperature, were calculated.

3.8.1. Hypoxanthine^{2-} monoprotonation

Table 3(b) shows the respective hypoxanthine^{2-} monoprotonation $\Delta\bar{G}$ values, involving several electron-donor sites. From these values, the hypoxanthine thermodynamic instability in its highest deprotonation level is found. This instability increases with temperature. On the contrary, the same trend between the monoprotonation $\Delta\bar{G}$ values and the, respectively, resulting monoanionic tautomers energetic stability is found. This is, the hypoxanthine^{2-} monoprotonation spontaneity increases with the resulting monoanionic forms energetic stability. This spontaneity also increases with temperature. Besides this, the suggested theoretical thermodynamic stability

Table 3
(a) Constants of tautomeric equilibria (tautomer K1⇔tautomer *i*) at 298.15 and 480.15 K for the hypoxanthine^{1-} tautomers in the gas phase. (b) $\Delta\bar{G}$ (kcal/mol) values at 298.15 and 480.15 K for the hypoxanthine^{2-} monoprotonation in gas phase, involving three different electron-donor sites, and (c) $\Delta\bar{G}$ (kcal/mol) values at 298.15 and 480.15 K for the two energetically most stable hypoxanthine^{1-} tautomers monoprotonation in gas phase

(a) Tautomer *i*	K_{eq}	
	298.15 K	480.15 K
K7	1.88×10^{-3}	2.05×10^{-3}
EOt	1.17×10^{-3}	9.72×10^{-4}
EOc	1.03×10^{-4}	8.49×10^{-5}
K9	1.40×10^{-5}	1.87×10^{-5}
K3	1.99×10^{-6}	2.69×10^{-6}
(b) Resulting monoanionic tautomer	$\Delta\bar{G}$ (kcal/mol)	
	298.15 K	480.15 K
K1	−431.89	−696.07
K7	−428.18	−690.17
EOt	−427.89	−689.46
(c) Resulting neutral tautomer	$\Delta\bar{G}$ (kcal/mol)	
	298.15 K	480.15 K
K17 (from K1)	−330.30	−532.34
K17 (from K7)	−334.02	−538.24
K19 (from K1)	−329.56	−531.17

(towards $\underline{H}^+$) descending sequence for the hypoxanthine^{2-} electron-donor sites here explored is found as follows: $\underline{N}(1) > \underline{N}(7) > \underline{O}$.

3.8.2. Hypoxanthine^{1-} monoprotonation

Table 3(c) shows the monoprotonation $\Delta\bar{G}$ values for the two energetically most stable hypoxanthine^{1-} forms. The hypoxanthine^{1-} thermodynamic instability arises at a lower level than that for hypoxanthine^{2-}. Although we selected few processes, the same trend found before between the $\Delta\bar{G}$ values and the resulting neutral tautomers [19] (and starting from the same monoanionic form) energetic stabilities is observed. When the $\Delta\bar{G}$ values of Table 3(c) and the ones for other hypoxanthine^{1-} monoprotonation processes are considered, the suggested theoretical thermodynamic stability (towards $\underline{H}^+$) descending sequence for the hypoxanthine^{1-} electron-donor $\underline{N}$ sites is as follows: $\underline{N}(1) > \underline{N}(9) \approx \underline{N}(7) > \underline{N}(3)$. Interestingly, this sequence is in full agreement with the experimental studies on the tautomerism of neutral hypoxanthine in solution [17,18]. From these, the heterocycle in its $\underline{N}(1)$–H/$\underline{N}(7)$–H and $\underline{N}(1)$–H/$\underline{N}(9)$–H tautomeric forms has been deduced. Also, the suggested sequence is in full agreement with the hypoxanthine experimental protonation pattern in aqueous solution [6,7–16,41] and in solid state [6,35–38]. Analogous theoretical calculations on cationic hypoxanthine [34,39,40] give the same sequence, incorporating the $\underline{O}$ site as the one with the lowest protonic affinity. This suggestion is also in full agreement with the experimental studies quoted above.

3.9. IR vibrational spectroscopy

As part of the theoretical study, the respective IR vibrational spectrum calculation for both each one of the monoanionic tautomers and hypoxanthine^{2-} was carefully done. Also, the correspondent absorptions assignment was carried out.

For the theoretical IR vibrational spectrum calculation of hypoxanthine^{1-} in the gas phase at low temperature (as a theoretical reference for the experimental IR vibrational spectroscopy, which employs samples in an inert matrix), some assumptions were made. We considered that an abrupt experimental decrease in the gas temperature overcomes the tautomeric equilibria dynamics. Thus, we have selected the experimental [32] neutral hypoxanthine sublimation

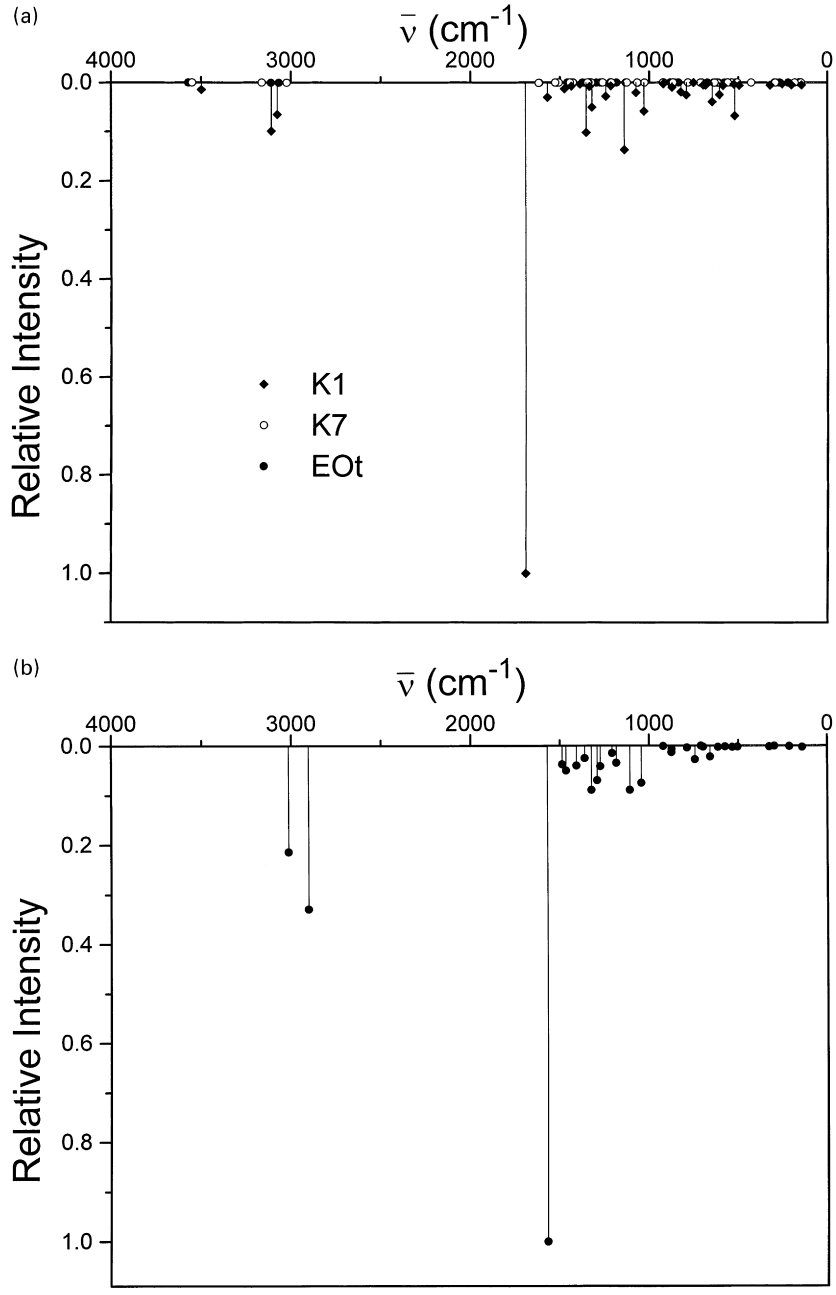

Fig. 5. Theoretical IR vibrational spectrum of: (a) hypoxanthine^{1-} in the gas phase, considering the relative contribution at 480.15 K of the three energetically most stable K1, K7 and EOt tautomers, and (b) hypoxanthine^{2-} in the gas phase.

temperature (480.15 K) as a more realistic value for which the monoanionic tautomers relative population analysis in the gas phase should be done. At these conditions, the relative population employed was the one that corresponds to the tautomeric equilibria at 480.15 K, and for which the respective tautomeric constants have been previously obtained (Section 3.7). The mole fraction x_i for each tautomer was

Table 4
Corrected wave numbers ($\bar{\nu}$, cm^{-1}), intensities (kM/mol) and vibrational modes assignment for: (a) the hypoxanthine^{1-} K1 tautomer, and (b) hypoxanthine^{2-}

$\bar{\nu}$ (cm^{-1})	I (kM/mol)	Assignment
(a)		
3498.48	10.36	ν (N(1)–H)
3109.69	71.74	ν (C(8)–H)
3076.35	47.24	ν (C(2)–H)
1692.21	724.81	ν (C=O), rings vib, N(1)–H vib
1569.28	21.82	rings vib, C(2)–H vib, ν (C=O)
1474.68	9.36	rings vib, C(8)–H vib, C(2)–H vib, ν(C=O)
1435.71	5.19	rings vib, C(2)–H vib, ν (C=O), N(1)–H/C(8)–H vib
1387.70	2.29	rings vib, N(1)–H vib, ν (C=O)
1354.05	73.76	rings vib, C(8)–H vib, C=O vib
1335.33	6.05	rings vib, C(2)–H vib, N(1)–H/C(8)–H vib
1321.59	36.66	rings vib, C(2)–H/C(8)–H vib
1244.41	20.35	rings vib, N(1)–H vib, C=O vib
1215.90	4.93	rings vib, N(1)–H/C(8)–H vib, ν (C=O)
1141.19	99.17	rings vib, C(8)–H vib
1074.85	14.78	rings vib, N(1)–H vib
1030.47	42.27	rings vib, C(2)–H vib
920.79	1.84	rings vib
873.01	7.18	rings vib
822.08[a]	13.96	C(8)–H vib
791.72[a]	18.29	C(2)–H vib, rings vib
751.37[a]	0.08	C(2)–H vib, rings vib, C=O vib
697.54[a]	3.53	N(1)–H vib, rings vib, C=O vib
683.77	3.68	rings vib
646.80[a]	28.28	rings vib, C=O vib
606.04[a]	17.76	N(1)–H vib, rings vib
584.96	4.35	rings vib, C=O vib
524.23	2.44	rings vib, C=O vib
520.73[a]	49.23	N(1)–H vib, rings vib
494.90	4.36	rings vib
321.34	3.89	C=O vib, rings vib
253.68[a]	2.00	rings vib
201.70[a]	3.37	rings vib
144.43[a]	3.58	rings vib, C=O vib

Table 4 (*continued*)

$\bar{\nu}$ (cm^{-1})	I (kM/mol)	Assignment
(b)		
3014.74	165.03	ν(C(8)–H)
2903.50	253.98	ν(C(2)–H)
1570.46	771.93	ν(C=O), rings vib
1487.48	28.92	rings vib, C(2)–H vib, ν(C=O)
1465.31	38.55	rings vib, C(8)–H vib, C(2)–H vib, δ (C=O)
1407.27	30.70	rings vib, C(8)–H vib, C(2)–H vib, C=O vib
1361.67	19.42	rings vib, C(2)–H vib, C(8)–H vib, ν (C=O)
1324.58	68.92	rings vib, C(2)–H vib, C(8)–H vib, C=O vib
1291.94	53.92	rings vib, C(2)–H vib, C=O vib, C(8)–H vib
1274.66	31.99	rings vib, C(2)–H/C(8)–H vib, C=O vib
1208.10	11.41	rings vib, C(8)–H vib
1184.51	26.77	rings vib, C(8)–H vib, ν (C=O)
1108.69	68.80	rings vib, C(8)–H vib, C=O vib
1043.83	57.92	rings vib, C(2)–H vib, C=O vib
920.50	0.80	rings vib, C=O vib
874.72[a]	10.36	C(2)–H vib, rings vib, C=O/C(8)–H vib
873.17	5.03	rings vib, C=O vib
787.06[a]	2.97	rings vib, C(2)–H vib, C=O vib
743.00[a]	21.23	C(8)–H vib, rings vib, C(2)–H/C=O vib
709.44[a]	0.03	rings vib, C=O vib
696.55	1.67	rings vib, C=O vib
657.86[a]	17.13	rings vib, C(8)–H vib, C=O vib
612.81	2.05	rings vib, C=O vib
573.56[a]	1.14	rings vib, C(2)–H vib, C=O vib
533.02	1.93	rings vib, C=O vib
503.59	1.38	rings vib, C=O vib
324.67	1.37	rings vib, C=O vib
296.83[a]	0.28	rings vib, C=O vib
211.97[a]	0.80	rings vib
139.39[a]	2.10	rings vib, C=O vib

[a] Means out of the molecular plane vibrations.

obtained from the K_{eq} values. The theoretical absorptions intensities in each IR spectrum were weighted by the correspondent mole fraction. After this, all the intensities were scaled referred to the highest intensity signal. The resulting theoretical hypoxanthine^{1-} IR spectrum in the gas phase is shown in Fig. 5(a).

From the figure, the K1 absorptions predominant contribution to the IR spectrum is deduced. Both the K7 and the EOt absorptions have no significant contributions. As consequence of the non-significant K_{eq} values differences for those tautomers with temperature, the IR spectrum which considers the tautomeric population at 298.15 K is the same as that shown in Fig. 5(a).

When this theoretical IR spectrum is compared with the theoretical ones that correspond to neutral [19] and cationic [34,39,40] hypoxanthine at the same sublimation temperature, several differences

arise. These could help to explore hypoxanthine either in its monoanionic, neutral or cationic states. One of such differences is the wave number values ($\bar{\nu}$, cm^{-1}) of the absorptions mainly attributed to the ν(C=O) vibrational mode. For these, the following $\bar{\nu}$ increasing trend with the heterocycle protonation level is found: hypoxanthine^{1-}K1(1692.21) < hypo-xanthine^{0}K17(1735.02) < hypoxanthine^{0}K19 (1755.79) < hypoxanthine^{1+}K179(1774.99) < hypoxanthine^{2+}K1379(1835.29). Fig. 5(b) shows the theoretical hypoxanthine^{2-} IR vibrational spectrum. Also here, several differences between this spectrum and the ones quoted above are detected. One of these is also for the highest intensity absorption, mainly assigned to the ν(C=O) mode. In this case it appears at 1570.46 cm^{-1}, and it is in full concordance with the theoretical $\bar{\nu}$ theoretical trend commented before.

In Table 4, the theoretical absorptions assignment for K1 and hypoxanthine^{2-} is presented.

In summary, the theoretical IR spectral features of hypoxanthine in the gas phase at different protonation states, and thus tautomeric and isomeric forms, could have diverse potential implications. Among these, the detailed theoretical analysis of the heterocyclic vibrational spectroscopy is outstanding. Also, this theoretical background would contribute to the analysis of some experimental physicochemical properties of the heterocycle obtained in the gas phase. Finally, some spectral features could be employed to explore the protonation state, the tautomeric or isomeric form, and the coordination mode of the heterocycle in its chemical interactions with Lewis acids in condensed matter.

4. Conclusions

From this study, the following conclusions can be drawn:

1. The relative energetic stability of certain hypoxanthine monoanionic forms depends on the basis set and functional used in the calculation. However, the total molecular energy analysis let us suggest the comparatively higher stability of the N(1)–H ketonic form. This N–H group also exists in the two energetically most stable (N(1)–H/N(7)–H and N(1)–H/N(9)–H) ketonic tautomers of neutral hypoxanthine. From this, the first protonic dissociation step of neutral hypoxanthine in the gas phase, could be suggested to be characterized by the comparatively higher population of the N(1)–H (K1) form in the resulting monoanionic heterocycle. Besides this, the N(1) site would be the predominant atom involved in the additional protonic dissociation of hypoxanthine^{1-}. The comparatively higher stability of K1 has also been inferred from experimental studies on hypoxanthine^{1-} in aqueous solution.
2. All the anionic forms are planar. Both the structural and the valence-occupied parameters, and also de TECD features are very sensitive to the tautomeric form and anionic level. The theoretical values for those properties let us suggest the existence of endocyclic regions associated with a double-bond character, their molecular distribution depending of the tautomeric form. The structural parameters here found show analogous trends as those obtained in experimental studies on hypoxanthine systems in the solid state.
3. The MEP and EDM vector properties are also strongly dependent of both the heterocyclic anionic level and its tautomeric form. Those properties could have implications in the potential heterocyclic reactivity weighted (or directed in the initial steps) by electrostatic interactions. Interestingly, those properties for the N(1)–H tautomer would imply that the N(7) and N(9) atoms would be potential favorable sites in attractive electrostatic interactions towards H^{+}. Indeed, these N sites (together with the N(1) atom) are the, respectively, protonated ones in the most predominant tautomeric forms of neutral hypoxanthine in solution. These N sites are also simultaneously protonated in hypoxanthine^{1+} either in aqueous solution or in the solid state. The comparatively higher energetic stability of hypoxanthine^{1+} in the N(1)–H/N(7)–H/N(9)–H ketonic form has also been recently inferred from theoretical studies.
4. From the frontier MOs properties, the molecular localization of the potential π-type Lewis base sites is suggested to be independent of the heterocyclic protonation level and tautomeric form. In this suggestion, the most stable forms of neutral and cationic hypoxanthine are included. The frontier MOs energies let us suggest the following qualitative ascending sequence of reductor of

character for the respective most stable forms: hypoxanthine^{3+} < hypoxanthine^{2+} < hypoxanthine^{1+} < hypoxanthine^{0} < hypoxanthine^{1-} < hypoxanthine^{2-}. This appears to be in agreement with the reactivity experimentally shown by the heterocycle towards Lewis acids.

5. The first vertical IP and EA values are also dependent of the heterocyclic tatuotmeric form and protonation level, and are in general agreement with the respective HOMO and LUMO energies. Both the IP and EA values support, respectively, the reductor/oxidant sequences suggested before. In these Redox processes the heterocyclic electron-donor and electron-acceptor properties are mainly associated with the π-type frontier MOs.
6. The constants of the tautomeric equilibria at 298.15 and 480.15 K for hyproxanthine^{1-} let us suggest the predominant contribution of K1 in the relative tautomeric population in the gas phase. Those theoretical results would support again the experimental suggestion concerning the predominant contribution of K1 to the hypoxanthine^{1-} tautomeric population in aqueous solution.
7. The $\Delta\bar{G}$ values for the protonation processes of hypoxanthine^{n-} let us suggest the spontaneity of these phenomena. This decreases with the step-by-step heterocyclic protonation. The $\Delta\bar{G}$ values analysis makes it possible to suggest differential σ-type basicities (towards $\underline{H}^{+}$) of the heterocyclic potential electron-donor sites. Independently of the deprotonation state, the $\underline{N}$(1) site is associated with the comparatively highest basicity; the $\underline{N}$ atom associated with the lowest protonic affinity is the $\underline{N}$(3) site. Among all the potential electron-donor sites, the exocyclic 0 site is suggested to show the lowest basicity. These theoretical suggestions appear again to be in agreement with the experimental Hypoxanthine-H^{+} equilibria.
8. The K_{eq} values were employed to obtain the relative contribution of the tautomers to the theoretical IR vibrational spectrum of hypoxanthine^{1-} in the gas phase. The $\underline{N}$(1)–H form is the predominant one. An exhaustive characterization of its absorptions was performed. The IR vibrational spectrum of hypoxanthine^{2-} was also obtained and characterized. The IR spectral features of the most stable forms of hypoxanthine in different deprotonation states would contribute to study some aspects of physicochemical and chemical processes of this heterocycle both in the gas phase and in condensed matter.

Acknowledgements

The authors are indebted to DGSCA, UNAM for the computer services facilities. This study was partially supported by DGAPA-UNAM, through Grant No. ES100597.

References

[1] M.N. Hughes, The Inorganic Chemistry of Biological Processes, 2nd edn, Wiley, New York, 1981.
[2] L. Stryer, Biochemistry, 3rd edn, Freeman, New York, 1988.
[3] T.G. Spiro (Ed.), Nucleic Acid–Metal Ion Interactions, 1, Wiley, New York, 1980.
[4] J.R. Lusty (Ed.), CRC Handbook of Nucleobase Complexes, Vol. I, CRC Press, Boca Raton, FL, 1990.
[5] J.S. Kwiatkowski, T.J. Zielinski, R. Rein, in: P.O. Löwdin (Ed.), Advances in Quantum Chemistry, Vol. 18, Academic Press, New York, 1986, p. 85.
[6] R. Acevedo-Chávez, M.E. Costas, R. Escudero, Inorg. Chem. 35 (1996) 7430, and references therein.
[7] D.J. Brown, S.F. Mason, J. Chem. Soc. (1975) 682.
[8] J.J. Christensen, J.H. Rytting, R.M. Izatt, Biochemistry 9 (1970) 4907.
[9] R.M. Izatt, J.J. Christensen, J.H. Rytting, Chem. Rev. 71 (1971) 439.
[10] D. Lichtenberg, F. Bergmann, Z. Neiman, Isr. J. Chem. 10 (1972) 805.
[11] P.W. Linder, M.J. Stanford, D.R. Williams, J. Inorg. Nucl. Chem. 38 (1976) 1847.
[12] R.L. Benoit, D. Boulet, L. Séguin, M. Fréchette, Can. J. Chem. 63 (1985) 1228.
[13] R.L. Benoit, M. Fréchette, Can. J. Chem. 63 (1985) 3053.
[14] R.L. Benoit, M. Fréchette, Thermochim. Acta 127 (1988) 125.
[15] R. Tauler, J.F. Cid, E. Casassas, J. Inorg. Biochem. 39 (1990) 277.
[16] E. Casassas, R. Gargallo, I. Giménez, A. Izquierdo-Ridorsa, R. Tauler, J. Inorg. Biochem. 56 (1994) 187.
[17] B. Pullman, A. Pullman, Adv. Heterocyclic Chem. 13 (1971) 77, and references therein.
[18] M.T. Chenon, R.J. Pugmire, D.M. Grant, R.P. Panzica, L.B. Townsend, J. Am. Chem. Soc. 97 (1975) 4636.
[19] M.E. Costas, R. Acevedo-Chávez, J. Phys. Chem. A101 (1997) 8309, and references therein.
[20] A.D. Becke, Phys. Rev. A 38 (1988) 3098.
[21] J.P. Perdew, Phys. Rev. B 33 (1986) 8822.

[22] N. Godbout, D.R. Salahub, J. Andzelm, E. Wimmer, Can. J. Chem. 70 (1992) 560.
[23] M.J. Frisch, G.W. Trucks, H.B. Schlegel, P.M.W. Gill, B.G. Johnson, M.A. Robb, J.R. Cheeseman, T. Keith, G.A. Petersson, J.A. Montgomery, K. Raghavachari, M.A. Al-Laham, V.G. Zakrzewski, J.V. Ortiz, J.B. Foresman, J. Cioslowski, B.B. Stefanov, A. Nanayakkara, M. Challacombe, C.Y. Peng, P.Y. Ayala, W. Chen, M.W. Wong, J.L. Andres, E.S. Replogle, R. Gomperts, R.L. Martin, D.J. Fox, J.S. Binkley, D.J. Defrees, J. Baker, J.P. Stewart, M. Head-Gordon, C. Gonzalez, J.A. Pople, GAUSSIAN 94, Revision D.4, Gaussian Inc., Pittsburgh, PA, 1995.
[24] S.S. Xantheas, J. Am. Chem. Soc. 117 (1995) 10373.
[25] J. Morrison-Galbraith, H.F. Schaefer III, J. Chem. Phys. 105 (1996) 862.
[26] G.S. Tschumper, H.F. Schaefer III, J. Chem. Phys. 107 (1997) 2529.
[27] R.J. Hall, N.A. Burton, I.H. Hillier, P.E. Young, Chem. Phys. Lett. 220 (1994) 129.
[28] M.J. Frisch, G.W. Trucks, H.B. Schlegel, P.M.W. Gill, B.G. Johnson, M.W. Wong, J.B. Foresman, M.A. Robb, M. Head-Gordon, E.S. Replogle, R. Gomperts, J.L. Andres, K. Raghavachari, J.S. Binkley, C. Gonzalez, R.L. Martin, D.J. Fox, D.J. Defrees, J. Baker, J.P. Stewart, J.A. Pople, GAUSSIAN 92/DFT, Revision F.3, Gaussian Inc., Pittsburgh, PA, 1993.
[29] UNICHEM 3.0, Cray Research, Inc., Eagan, MN, 1995 and XMOL, Version 1.3.1, Minnesota Supercomputer Center, Minneapolis, MN, 1993.
[30] DGAUSS 3.0.1/UC-3.0, Cray Research, Inc., Eagan, MN, 1991.
[31] I. Mayer, Int. J. Quantum Chem. 29 (1986) 477.
[32] G.G. Sheina, S.G. Stepanian, E.D. Rádchenko, Yu.P. Blagoi, J. Mol. Struct. (Theochem) 158 (1987) 275.
[33] D.A. McQuarrie, Statistical Mechanics, Harper and Row, New York, 1973.
[34] M.E. Costas, R. Acevedo-Chávez, J. Mol. Struct. (Theochem) 489 (1999) 73.
[35] J. Sletten, L.H. Jensen, Acta Cryst. B 25 (1969) 1608.
[36] M.R. Caira, L.R. Nassimbeni, A.L. Rodgers, Acta Cryst. B 31 (1975) 1112.
[37] R.D. Rosenstein, M. Oberding, J.R. Hyde, J. Zubieta, K.D. Karlin, N.C. Seeman, Cryst. Struct. Comm. 11 (1982) 1507.
[38] H. Schmalle, G. Hänggi, E. Dubler, Acta Cryst. C46 (1990) 340.
[39] M.E. Costas, R. Acevedo-Chávez, J. Mol. Struct. (Theochem) 468 (1999) 39.
[40] M.E. Costas, R. Acevedo-Chávez, Density functional study of the tricationic hypoxanthine isomeric forms, in preparation.
[41] R. Acevedo-Chávez, M.E. Costas, Polyhedron 18 (1999) 1549.